Engineering of Hexagonal Microtextures on Glass

Padmakumar, Govind; Balaji, Aravind; Criel, Matthias; Saitta, Federica; Limodio, Gianluca; Perez-Rodriguez, Paula; van Swaaij, René A.C.M.M.; Smets, Arno H.M.

DOI
10.1021/acsaom.5c00328

Publication date
2025

Document Version
Final published version

Published in
ACS Applied Optical Materials

ACS APPLIED OPTICAL MATERIALS

pubs.acs.org/acsaom

Article

Engineering of Hexagonal Microtextures on Glass

Govind Padmakumar,* Aravind Balaji, Matthias Criel, Federica Saitta, Gianluca Limodio, Paula Perez-Rodriguez, René A. C. M. M. van Swaaij, and Arno H. M. Smets

Cite This: *ACS Appl. Opt. Mater.* 2025, 3, 2360−2372

Read Online

ACCESS | Metrics & More | Article Recommendations

ABSTRACT: Textured glass is used in a wide range of applications to improve optoelectrical performances, such as photovoltaics, biosensing, microfluidics, and photonics. Honeycomb textures have demonstrated an excellent performance in optical devices using crystalline silicon wafers as opaque substrates. As a pathway to translate these advantages to configurations implementing glass, hexagonal-shaped microsized craters (honeycombs) are made on glass in this study. We use photolithography combined with wet etching for this process. The relationship between photoresist mask design, glass−photoresist adhesion, wet-etching steps, and the mechanism of honeycomb formation is studied. It is demonstrated that the higher the isotropic nature of etching achieved, the deeper the hexagonal craters will be. The potential of hexagonal textures on glass to significantly reduce reflection to <8% over the entire spectral range is observed. Finally, hexagonal microsized textures with 5 μm periodicity and 1.01 μm depth that effectively diffuse 50% of the total transmitted light at near-infrared (1100 nm) wavelengths are developed.

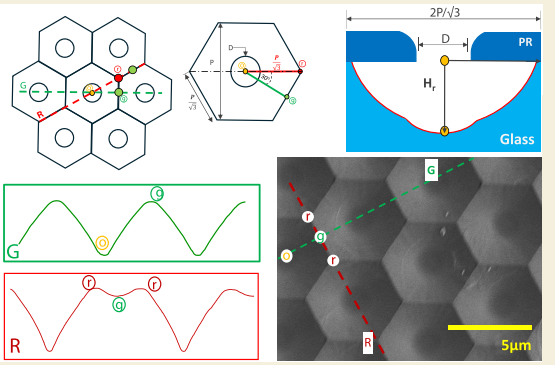

KEYWORDS: *glass texturing, photolithography, hexagonal textures, honeycombs, diffused transmission*

INTRODUCTION

Texturing of glass is extensively used in applications in which active interaction with light is required. In photovoltaic (PV) applications, textured glass surfaces enhance light trapping to improve efficiency; in biosensing, textures on glass improve sensitivity and detection capabilities;[1,2] in photonics, textures manipulate light, generating colors and adding haze;[3−5] in microfluidics, textures make channels for devices.[6] Two broad classifications of textures are (i) random shapes with a random distribution over the surface and (ii) periodically distributed shapes on the surface.

Wet etching with a deposited crystalline sacrificial layer is an effective method to develop random textures on glass. The crystals over glass act as a selective mask to form craterlike structures on glass. This "leaking" mask is partly or wholly removed during a chemical wet-etching process step.[7,8] The etching solution penetrates the easiest through pinholes and pores around the grain boundaries in the layer. As the sacrificial layer is dissolved, the glass is inhomogeneously etched, resulting in a random texture at the surface.[9,10]

To make a periodic texture on any surface, the constituent geometric shape should cover the plane with no gaps or overlaps. This property is called tessellation. The three regular polygons that can form regular tessellation are triangles, squares, and hexagons.[11] Regular hexagons have the smallest perimeter for a given area among all shapes that can tessellate. This property, referred to as "honeycomb conjecture", makes hexagons the most efficient shape for enclosing and separating spaces.[12] For crystal depositions, honeycomb-shaped textures minimize the length of sharp boundaries caused by texture borders, which can otherwise interfere with the crystal structure, causing cracks.[13] For this reason, hexagonal textures (alias 'honeycomb textures') are of special interest in thin-film PV applications. Commonly adopted methods to make periodic hexagonal textures are nanoimprint lithography (NIL),[14] laser ablation,[15] and photolithography.[16] NIL is a method of physically pressing a polydimethylsiloxane (PMDS) mold with a targeted pattern onto a substrate coated with a thin polymer layer. The polymer layer with the impressed pattern is cured under ultraviolet (UV) light as the next step. Upon removal of the PMDS stamp, the complementary pattern is made on the substrate.[17,18] A nanoimprinted resist layer can also be used as a three-dimensional etching mask to obtain a hexagonal pattern in the c-Si absorber surface by reactive ion etching.[19] To make hexagons on metals, laser ablation is utilized. A nanopulsed fiber laser beam travels in a

Received: July 31, 2025
Revised: September 23, 2025
Accepted: September 26, 2025
Published: October 1, 2025

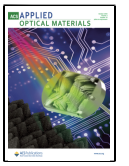

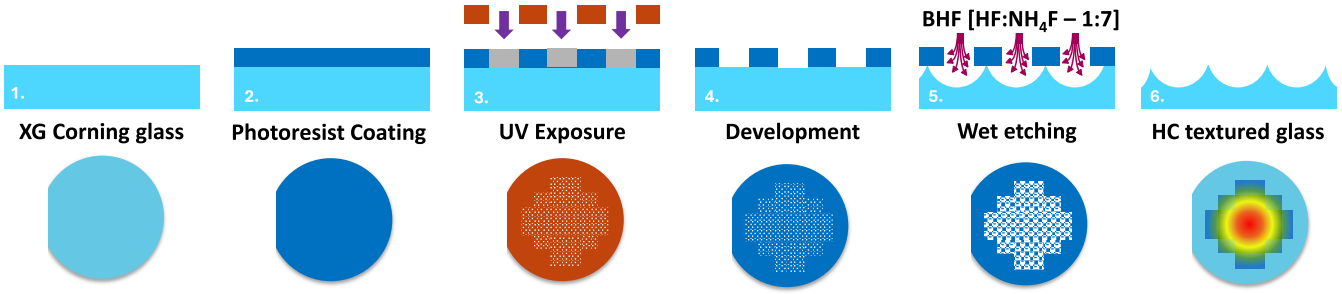

Figure 1. Schematic diagram of all steps involved in generating hexagonal textures on glass (top row). The bottom row shows Corning glass wafers after the corresponding steps.

hexagonal pattern on the substrate surface to remove a material partially through vaporization or sublimation.[20]

Photolithography uses polymer-based materials known as photoresists (PRs). The PR layer clones a desired pattern with the help of either X-ray or UV light transmitted through a photomask.[21] When exposed to these high-energy wavelengths, the PR degrades. These degraded areas are removed in the following step called "development". In the final step of pattern generation, the glass substrate with PR masks is dipped in an etchant to remove the material from its surface. Since PR-covered regions act as a shield for etching, selective etching through the PR-less areas creates patterns on the substrate. Photolithography is generally used to make patterns on silicon wafers.[22,23] Lithography with row-wise distributed and alternatively spaced orifices for wet etching can make hexagonal patterns.[24,25] In this method, a silicon dioxide (SiO_2) layer is grown on the wafer surface and subsequently patterned with orifices. The wafer is subsequently wet-etched isotropically using an acid solution (HNO_3:HF:CH_3COOH—25:1:10) or BHF to obtain hexagonal features.[13,26−28] Texturing methods on glass differ from texturing on silicon wafers. Glass is an amorphous solid with a random network of silicon and oxygen atoms.[29] To develop honeycomb textures on glass wafers, a similar photolithography mask technique can be employed. This can be done without an additional SiO_2 layer.[30,31] However, upon direct translation of photolithography and subsequent etching steps to glass, the resultant textures suffer from flat bottom regions.[32] The detailed optimization of the steps involved in photolithography to create honeycomb textures on glass has not yet been explored. Hexagonal textures with flat bottom regions cannot actively scatter light itself and require additional scattering mechanisms[33] when used in PV applications.

The work presented in this article aims to develop a fabrication process for making honeycomb textures on glass with rounded bases. We have taken the process of making honeycomb textures on silicon[13] as a starting point and optimized it to achieve the desired rounded features on glass. For the first time, this article identifies challenges specific to developing honeycomb textures on glass using photolithography. The underlying wet-etching mechanism and its implications for the surface morphology are explored in detail. Further, process parameters based on the shape and height of the hexagons are optimized. We define the term 'effective orifice diameter' as a parameter to quantify the isotropism involved in the generation of hexagonal textures on glass. Finally, we demonstrate the potential of hexagonal textures on glass to enhance the total transmittance while ensuring excellent light scattering.

MATERIALS AND METHODS

Generating Hexagonal Textures on Glass

The methodology adopted to create hexagonal textures on glass is similar to that described in refs 13,34. The glass substrates used in this study are Corning glass XG Boro-alumino-silicate glass wafers of 4 in. in diameter and 0.7 mm thickness with a primary flat.[35,36] The basic process for obtaining the honeycomb textures using photolithography on glass superstrates is depicted in Figure 1. Each step in Figure 1 is detailed in the following subsections.

Step 1: Superstrate Preparation. The glass wafers are composed of silicon oxide, which makes them extremely hydrophilic. In Step 1, the glass wafer undergoes a nonacidic cleaning step to remove organic impurities from its surface. This includes 10 min of ultrasonic cleaning in an acetone bath followed by 10 min in an isopropyl alcohol bath.[37,38] The cleaned glass is dried with a nitrogen flow and loaded for further processing. It is essential to conduct these steps with minimal delay to prevent the hydroxyl groups from getting attached to the surface from the atmosphere.[38]

Step 2: Coating of the PR on the Superstrate. Following cleaning, the next step is to coat the PR layer onto the glass superstrate. An EVG120 coater machine is used for this step.

Precoating Bake. In a prebaking step inside the EVG120 coater, the substrate is annealed at 100 °C for 600 s. This is an extra step to decrease the surface density of the hydroxyl groups attached to the surface as much as possible.

Hexamethyldisilazane (HMDS) Exposure. After prebaking, the wafer is vapor-primed with HMDS on a hot plate in order to suppress any remaining hydroxyl groups. HMDS priming of the surface before coating the PR significantly affects PR adhesion on the surface.[38] The reaction between the OH group on the surface and the methyl groups boosts the hydrophobicity of the surface. HMDS forms a strong bond with hydroxyl groups on the wafer surface, thereby bridging the inorganic wafer and the organic photoresist.[38,39] The EVG120 coater exposes the samples to HMDS with N_2 as the carrier in a separate priming chamber. This process is carried out at 130 °C for 50 s.

PR Coating. The PR used in this work is a Shipley SPR3012 positive PR. A 1.4 μm thick SPR3012 is coated on glass. The coater tool dispenses 2600 μL of the PR at a rate of 1000 μL/s onto a wafer spinning at 600 rpm. Afterward, an acceleration of 2500 rpm/s is applied until the wafer reaches a rotational speed of 3450 rpm, which is maintained for 30 s. The resist can flow around the wafer edges, or the resist may splatter from the coater bowl, too. Both cases can land the PR on the back side of the glass wafer and can eventually cause issues in later processing steps (such as contaminating hot plates or introducing flatness errors during exposure). Then, the back side of the wafer is rinsed (BSR) with propylene glycol methyl ether acetate (PGMEA) for 2 s at a rotational speed of 1700 rpm. At the end of this step, the rotational speed increased to 2500 rpm to remove PGMEA.

Postcoating Bake. Once the PR is coated on the wafer, it is soft-baked (or baked postcoating) for 90 s at 90 °C. This step ensures that a monolayer of the PR is formed on the superstrate surface.[40] The formed monolayer ensures that the pattern's accuracy is maintained postdevelopment, aiding in the formation of a precise PR mask on the superstrate. The optimum annealing duration and temperature

https://doi.org/10.1021/acsaom.5c00328
ACS Appl. Opt. Mater. 2025, 3, 2360−2372

suggested in the technical datasheet offered by Merck[41] are used in the EVG120 recipe. This is conducted in a dedicated chamber at 90 °C for 90 s. Afterward, the wafer is cooled on a cooling plate for 20 s.

Step 3: Exposure of Coated Superstrates. The subsequent step after PR coating is exposure of the coated PR to UV light. The UV exposure is conducted using the ASML PAS5500/80 wafer stepper. For 1.4 μm thick PR-coated wafers, exposure is done at 150 MJ/cm^2. The chromium reticle used for obtaining hexagonal textures has a pattern of orifices spaced out at a particular periodicity along the horizontal direction. Around each orifice, six adjacent orifices are spaced out at 60° angles. Figure 2 shows an SEM image of this orifice distribution on the PR mask.

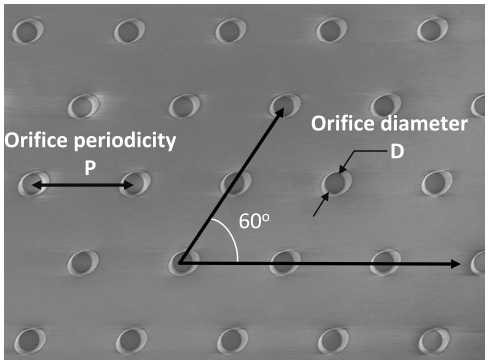

Figure 2. SEM image of the 2D distribution of orifices on the PR imparted using the chromium reticle.

Step 4: Development of Exposed Superstrates. In the final step of photolithography, the exposed superstrates are developed in the EVG120 developer. The superstrate is spun at 5 rpm in the developer rack with the developer solution poured onto the surface. The slow spin speed ensures a uniform layer of the developer solution, which reacts with the exposed parts of the PR and dissolves them. Then, the superstrate is spun at high speeds ranging from 2000 to 3000 rpm and washed with DI water to remove the dissolved PR from the wafer surface. At this step, the PR mask formation is complete with a diameter (D) of 1000 ± 11 nm and an orifice periodicity (P) of 3000 ± 13 nm. The standard deviations of D and P reported in this article are based on multiple measurements of the orifice diameter and periodicity after the development of the PR.

Hard Baking. Following this, the superstrate with the developed pattern is baked at 100 °C for 90 s to evaporate the excess PR and developer present on the superstrate. This step hardens the PR and causes cross-linking.

Step 5: Wet Etching of Patterned Superstrates. The glass superstrate with the patterned PR is to be chemically etched to obtain hexagonal texturing on the surface. This is done in a sequence of two steps. The first step involves a 1 min dip in a 1:5000 aqueous Triton X-100 ($[C_{14}H_{22}O(C_2H_4O)_n$:$H_2O$ = 1:5000]) bath. The main purpose of this bath is to improve the wettability of the surface by the etchant. Triton X-100 acts as a surfactant, lowering the surface tension and enabling better contact between the solid and the aqueous medium.[42]

In the next step, the glass wafer is dipped as a whole in the etchant to make patterns. The non-PR-coated side of the wafer is not shielded from etching during the process. For glass etching, hydrofluoric acid (HF) offers an etching rate of around 833 nm/min at a 40% concentration.[35,36,43] However, the usage of HF increases the peeling off of the PR due to the influx of the F^- ions through the PR.[44,45] To gain better control over the etching rate and etch step, in this work, we use premade buffered hydrofluoric acid (BHF), composed of ammonium fluoride (NH_4F) (40%):hydrofluoric acid (HF) (49%) in the ratio 7:1. In BHF, the buffer results in an increase in the concentration of F^- ions and due to their high electronegativity, it tends to form HF_2^- ions. The PR is more resistant to the diffusion of these ions due to their larger size. This helps to protect the PR from the impact of HF and aids in better selectivity in the etching of the glass.[44,45]

Step 6: Cleaning of Textured Superstrates. The remaining photoresist on the glass is removed with a PVA TePla Microwave Plasma system asher. The cleaned glass is dipped in ultrasonic baths of acetone, followed by isopropyl alcohol for 10 min each.[37,38] The cleaned glass is dried with a nitrogen flow.

Design of Experiments

Experiments in this work are conducted in three phases. An overview of the design of experiments is depicted in the flowchart shown in Figure 3. The crater height of a completely developed hexagon is the

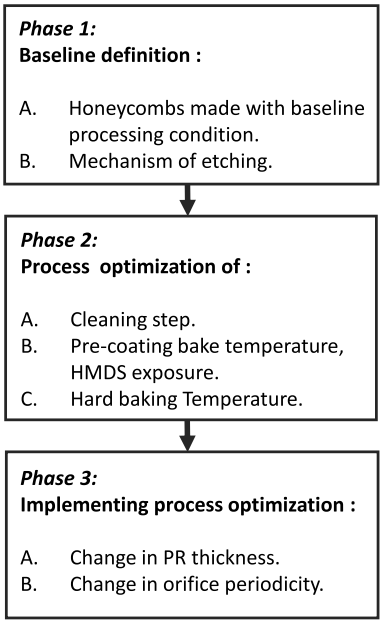

Figure 3. Flowchart of the design of experiments. The experiments in this manuscript are divided into three phases.

metric chosen to define the texture quality throughout the experiments. To clarify the term height of texture, Figure 4 is included.

Phase 1: Baseline Definition. To define a baseline for the processing conditions, with the processing steps elaborated in Section "Generating Hexagonal Textures on Glass", an etching duration series of 18 to 30 min with 2 min steps was conducted. This experiment was carried out to observe the properties of hexagonal textures on glass and to identify the challenges involved in processing.

Phase 2: Process Optimization. In this phase, the experiments are designed to optimize the processes involved in superstrate cleaning and preparation, coating of the PR on the superstrate, and development of exposed superstrates. The experiments in these three sections are optimized based on the adhesion between the PR and glass.

2.A. Four different cleaning procedures are attempted to identify a suitable surface cleaning procedure for photolithography on Corning XG glass: (i) nonacidic cleaning with IPA and acetone in an ultrasonic bath; (ii) acidic cleaning by dipping the wafers in an HNO_3 (30%) bath for 3 min at room temperature; (iii) acidic cleaning by dipping the wafers in HNO_3 (69.5%) at room temperature for 3 min; and (iv) acidic cleaning by dipping the wafers in an HNO_3 (99%) bath, followed by an HNO_3 (69.5%) bath for 3 min each. All baths used for cleaning have dimensions of 15 cm × 15 cm × 15 cm. HNO_3 was selected for its feasibility, as it is the standard cleaning solution available in the laboratory where these experiments were conducted. These wafers were cleaned in a deionized running water bath in each procedure. After rinsing, the samples were dried using the spin dryer. For each cleaning procedure, two wafers were coated with 1.4 μm PR

https://doi.org/10.1021/acsaom.5c00328
ACS Appl. Opt. Mater. 2025, 3, 2360−2372

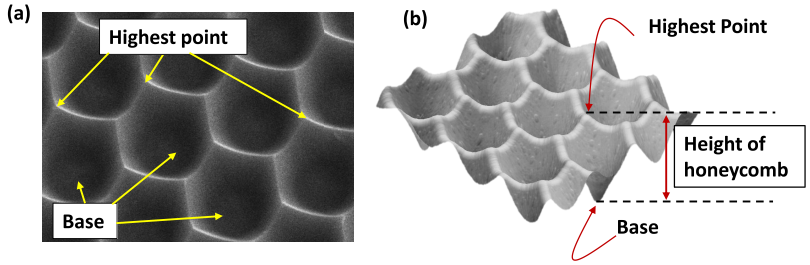

Figure 4. Image of a completely developed honeycomb. (a) SEM image (tilted view). (b) Concept of height of the honeycomb as defined in the text.

and wet-etched for 24 min, and their height was analyzed with atomic force microscopy (AFM) data.

2.B. To optimize the PR coating on the superstrate, a variation in the precoating bake temperature and HMDS exposure is conducted, staying within the limits of the EVG120 coater tool. The maximum duration for the prebaking was fixed at 10 min since the dipod arm in the EVG120 coater cannot handle hot superstrates. If the superstrates were to be heated longer, they had to be cooled again before being used in the EVG120 coater. This delay could offer enough time for the surface to readsorb water. To determine the optimum precoating bake temperature, the samples were heated at temperatures ranging from 100 to 140 °C, in 10 °C increments. This temperature range was suggested by the manual provided by Microchemicals for sample preparation.[40] The HMDS exposure time varies from 0 to 150 s in 50 s increments. For these two experiments, the hydrophobicity of the surface is studied to identify the influence of each step in PR adhesion on glass (the measurement procedure is described in the upcoming Section "Hydrophobicity of Glass Wafers").

2.C. To study the effect of the development steps, the influence of the hard-baking temperature is studied. Hard baking is generally done to physically and chemically stabilize the PR material. The thermal softening and roundening of PR3012 occurs at a temperature around 110−130 °C, called as the reflow temperature.[46,47] The two options considered for this experiment include hard baking at temperatures similar to and above the reflow temperature of the PR.[48] The first trial is to heat the superstrates at 110 °C for 30 min. The second option is hard baking the PR at 140 °C for 30 min. It was also necessary to etch the samples to visualize the effect of the hard-baking experiment. The samples were etched over an etching duration series conducted for 14 to 30 min at 2 min intervals. At each time value, one wafer was processed and etched. These samples were processed using optimized conditions obtained from sections "Influence of the Cleaning Method", "Influence of the Precoating Bake Temperature" and "Influence of the HMDS Exposure Duration". The physical properties of each wafer were studied by AFM scanning of multiple spots on the wafer to ensure the spatial uniformity of textures.

Phase 3: Implementing the Optimized Process. In Phase 3 of the experiments, the parameters optimized through the experiment conducted at Phase 2 are implemented. The experiments in Phase 3 do not impact Phase 2 as the conditions optimized in Phase 2 address the PR−glass adhesion, which is kept the same for Phase 3.

3.A. To study the effect of variation of the PR thickness, the thickness of PR SPR3012 is increased to 2.1 μm. An etching duration series for 14 to 26 min for each PR thickness is conducted. This work does not attempt to use a chemically different PR because such a change might require reoptimizing parameters explored in Phases 1 and 2. For a 2.1 μm thickness, a 3000 μL volume of PR is dispensed at 750 μL/s on a spinning wafer at 600 rpm. Then, an acceleration of 1000 rpm/s is introduced to reach a speed of 1575 rpm, which is kept constant for 30 s. The back side of the wafer is rinsed with PGMEA for 2 s at 1500 rpm. At the end of this step, the rotational speed increases to 2500 rpm to remove PGMEA. Since the UV exposure dose for a sample is determined based on the thickness of the PR used, a UV exposure dosage of 315 MJ/cm^2 is required for a 2.1 μm thick PR.

3.B. To study the effect of orifice periodicity on etching, PR masks corresponding to periodicities 3, 4, and 5 μm were used. An etching duration series between 14 and 24 min is made for each periodicity.

At each phase of this work, the observed patterns are physically correlated to the etching process utilizing matrices defined in the upcoming section. It has to be noted that the wafers were etched one at a time, as the author's attempts to etch multiple wafers simultaneously in one bath [dimension: 15 cm × 15 cm × 15 cm] had adverse effects on texture uniformity due to the redeposition of the peeled-off PR onto adjacent wafers.

Characterization Methodology

Hydrophobicity of Glass Wafers. The surface energy or hydrophobicity of the surface could be related to the contact angle of a water droplet dropped onto the surface. This could be measured from the superstrate's water contact angle (WCA). The WCA is the contact angle formed by a water droplet on the surface. This measurement is conducted with DataPhysics-OCA200. One μL of water was dropped on five different spots on the superstrate. The droplet's left and right contact angles with the superstrate are calculated with a microscopic image of the droplet profile as illustrated in Figure 5. The mean values of the five measurements indicate the hydrophobicity of the surface.

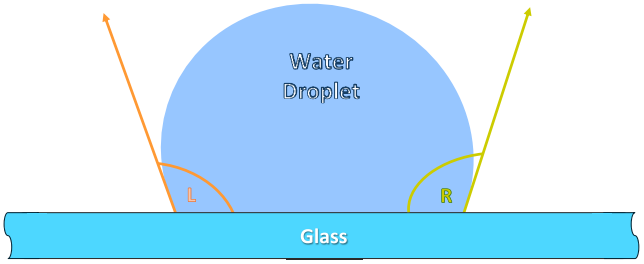

Figure 5. Illustration of the water contact angle measurement. L and R represent the tangential angles formed by water with glass at the left and right contact points.

Physical Characterization. To examine the surface morphology of developed textures with AFM, a Bruker AFM FastScan system with a FastScan closed loop scanner head is utilized. Scanning areas of 16 μm × 16 μm were chosen for analyzing the differently sized textures. The surface parameters, such as the maximum height and slope distribution, were extracted from the AFM data using Bruker's NanoScope Analysis software. The standard deviation in the height measurement of texture was reported based on multiple AFM measurements of the same wafer. The practical surface area analysis and angle distribution are completed using Gwyddion software (version 2.63). Gwyddion analyzes the surface slopes based on normalized occurrence curves of angles subtended by surface vectors with the vertical plane. The scanning electron microscopy (SEM) analysis of the surface was conducted on a Hitachi Regulus 8230 scanning electron microscope at an acceleration voltage of 1.5 kV.

Optical Characterization. Optical transmission measurements were carried out using a LAMBDA 1050+ UV/vis/NIR spectropho-

https://doi.org/10.1021/acsaom.5c00328
ACS Appl. Opt. Mater. 2025, 3, 2360−2372

tometer with a 150 mm InGaAs integrating sphere from PerkinElmer. All glass samples were probed with light on the flat side for this measurement. The percentage of light transmitted in any direction other than normal is quantified as diffused transmittance (T_D). T_D values at different wavelengths were considered the prime metric for quantifying the optical scattering performance in this work. The total transmission (T_{TOT}) and T_D of flat glass (acid-cleaned glass wafer) are also added as a reference.

RESULTS AND DISCUSSION

Mechanism of Etching

The different steps involved in forming hexagonal textures through wet etching are schematically illustrated in Figure 6.

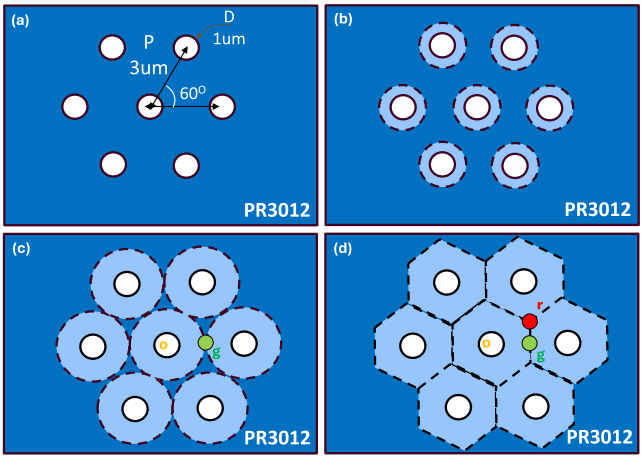

Figure 6. Demonstration of hexagon formation during etching with BHF. (a) Position and spacing of orifices to make hexagonal textures. (b) The initial etching stage is when BHF enters through the orifice and initiates crater propagation. (c) Initial intersection points of craters (green dot, marked as g). (d) Completion of honeycomb formation (red dot, marked as r).

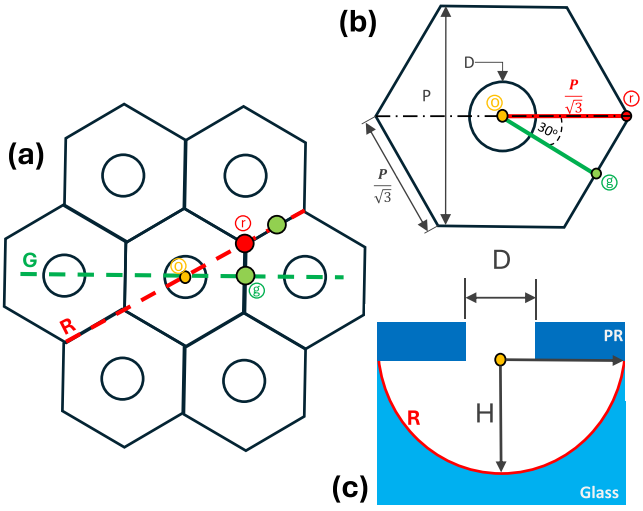

Figure 7. (a) Top view of hexagonal microtextures after final cleaning. (b) Dimensions of one hexagon unit in terms of periodicity, P. (c) Cross-sectional representation of etched glass with the PR assuming isotropic etching with BHF. The axes are marked R and G.

The circular patterns formed on the glass surface intersect to form a hexagon due to the spatial placement of orifices on the PR mask.

The center of the orifice can be considered the origin of the etching process, which is marked as "o" in Figure 6. The distance between the orifices on the PR is translated to the periodicity (P) of the resultant texture. The etchant penetrates through the orifice and etches glass vertically and laterally. The lateral etching exhibits a circular behavior centered at "o". The first intersection point of the formed circles is marked "g" in Figure 6c. The circle's boundary propagates radially outward and eventually merges with that of its neighbors, as demonstrated in Figure 6d. The point "r" marks the completion of merging and formation of hexagonal shapes. Removal of glass in the vicinity of "g" continues until the hexagon formation is completed. By geometry, "g" is at a distance of P/2 from the origin "o" and "r" is at a distance P/$\sqrt{3}$ from the origin "o". Figure 7a shows the schematic top view of hexagons on glass. Figure 7b shows the top view of a unit hexagon. The hexagons have an edge with a P/$\sqrt{3}$ length.

Physical Characterization of Textures

A regular hexagon is symmetric at 60° rotations and asymmetric at 30° rotations. The surface profile of wet-etched hexagonal textures differs in two directions, with a phase difference of 30°. Figure 7 explicitly shows the two directions. Two surface profiles in these directions can describe the entire surface topology of each hexagon. The two directions are named the Red axis (R-axis) and the Green axis (G-axis) for convenience. The G-axis represents an imaginary center-to-center line perpendicular to the edge of the hexagons. The R-axis represents the center-to-center line parallel to the edges of the hexagons. This is demonstrated in Figure 8a.

The height profile along the G- and R-axes is plotted on the same scale as shown in Figure 8b. The observed peak height of the R-axis (H_r) is more than that of the G-axis (H_g). Both profiles are periodic in nature, with periodicity P along the G-axis and periodicity 1.44 P along the R-axis. This arises from the fact that "r" marks the point of completion of the honeycomb and is located at a longer distance than "g" from "o".

From Figure 7b,c, for the isotropic etching mechanism, the expected texture height (H_{exp}) can be related to the orifice diameter (D) and texture periodicity (P) by the equation

$$H_{exp} = \frac{P}{\sqrt{3}} - \frac{D}{2} \quad (1)$$

Effective Orifice Diameter (D_e)

To quantify the extent of isotropism resulting from etching, we define the term effective orifice diameter (D_e). D_e for a specific periodicity is the orifice diameter at which the texture height is achieved by isotropic etching. A decrease in the numerical value of D_e signifies enhanced directional uniformity in the etching. For any peak height, H_r measured, D_e is given as

$$D_e = 2\left[\frac{P}{\sqrt{3}} - H_r\right] \quad (2)$$

The term $\sqrt{3}D_e/2P$ gives a ratio of the effective orifice diameter to the diagonal length of the honeycomb. This term will be referred to as $D_{e,P}$ from now on in this paper. $D_{e,P}$ can quantify the isotropism of a processing step, irrespective of texture periodicity. This term is also a measure of the texture's sensitivity toward a subprocess. The aspect ratio (AR) of hexagons on glass can be defined in terms of $D_{e,P}$ as

https://doi.org/10.1021/acsaom.5c00328
ACS Appl. Opt. Mater. 2025, 3, 2360−2372

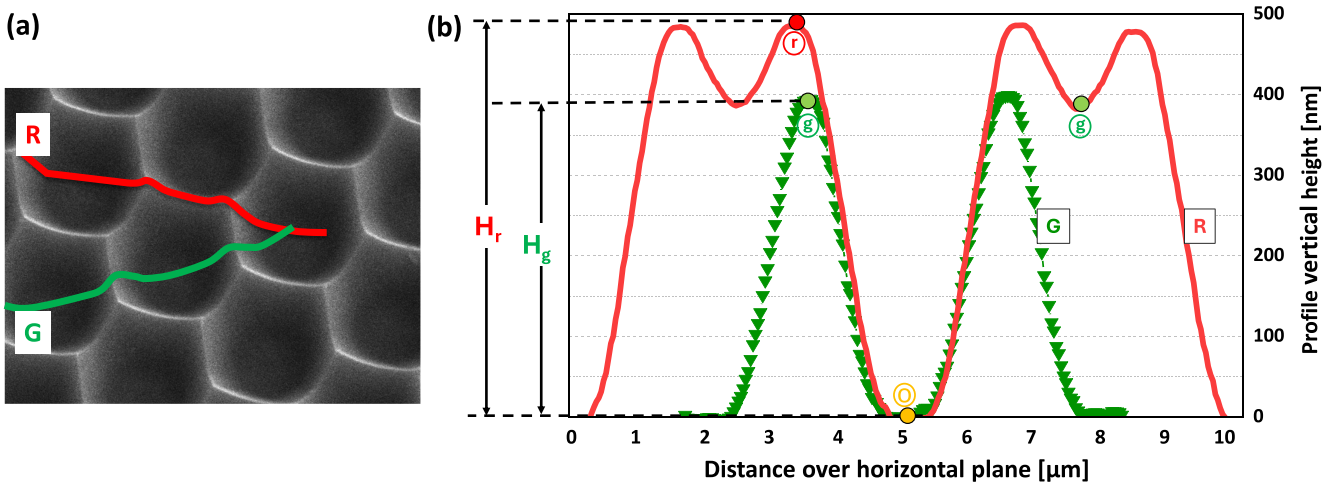

Figure 8. (a) Demonstration of the asymmetric axes (G- and R-axes) of the honeycomb texture (SEM image). (b) Extracted AFM profiles over the R-axis profile (solid line, marked R) and the G-axis profile (lines with triangles, marked G). Points with encircled letters are the same as those shown in Figure 7(a). The profiles are extracted from AFM data with a 3 μm periodic texture.

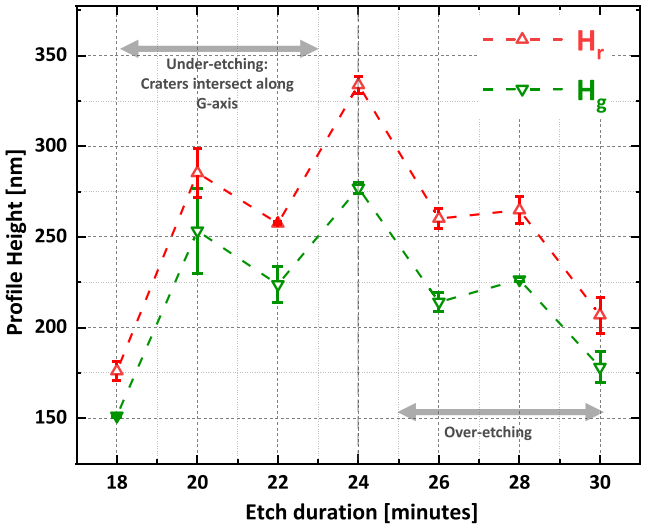

Figure 9. Profile height of the G-axis (green) and R-axis (red) for wafers processed with baseline conditions for different etch durations.

$$\mathrm{AR} = \frac{H_r}{P} = \frac{1}{\sqrt{3}}[1 - D_{e,P}] \tag{3}$$

Baseline Processing

The measured peak profile heights H_r and H_g with AFM are plotted against etching durations, as shown in Figure 9. As explained in Section 3.1, the lateral propagation of etching leads to the formation of hexagons. Once the circles join completely, honeycomb formation is complete. For baseline definition time series, this event occurs at 24 min. Glass wafers etched below this duration are underetched, and those etched above this duration are overetched.

The presented time series starts at 18 min. For etch durations below 18 min, the situation resembles Figure 6b. For this case, the heights of the two profiles are the same $H_r = H_g$. Above 18 min, the circles intersect along the G-axis, but are still distinct along the R-axis (as shown in Figure 6c). The SEM image shown in Figure 10 represents this scenario. From Figure 10b, it is clear that $H_r > H_g$ once etching starts at point "g". Both H_r and H_g increase with the etching duration up to 24 min and decrease if overetched. The highest value of H_r in this time series is 0.34 ± 0.01 μm when the hexagons are completely developed.

The value of $H_r - H_g$ increases over time and is the highest for completely developed hexagons (etch time = 24 min). Beyond 24 min, when overetched, etching at "r" is quicker than "g" as the conical structures at "r" are etched from all sides.

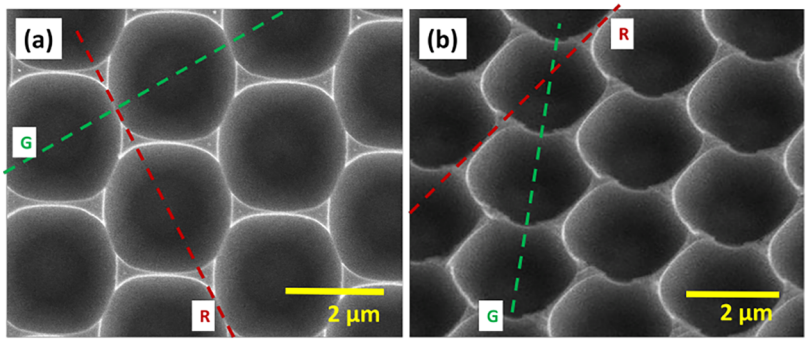

Figure 10. SEM images of the underetched glass wafer (corresponding to the etching time for 22 min, as shown in Figure 9). (a) Top view. (b) Tilted view.

https://doi.org/10.1021/acsaom.5c00328
ACS Appl. Opt. Mater. 2025, 3, 2360−2372

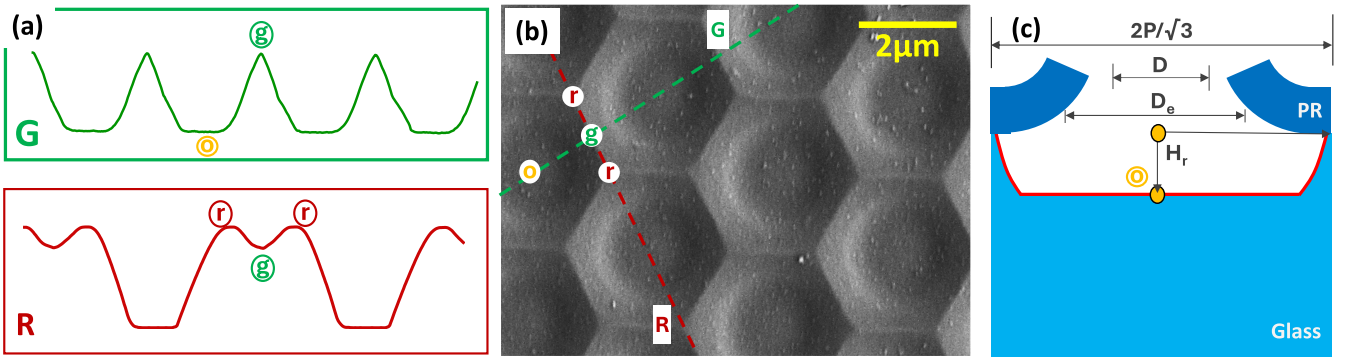

Figure 11. Three μm periodic hexagonal textures with a flat base. The sample corresponds to baseline processing conditions etched for 24 min. (a) 2D surface profile along the G- and R-axes as extracted from AFM (profiles are not to scale). (b) SEM image. The encircled letters are given to aid in the interpretation of the SEM image. (c) Conceptual drawing of the PR peel-off and the effective orifice diameter D_e leading to a flat base.

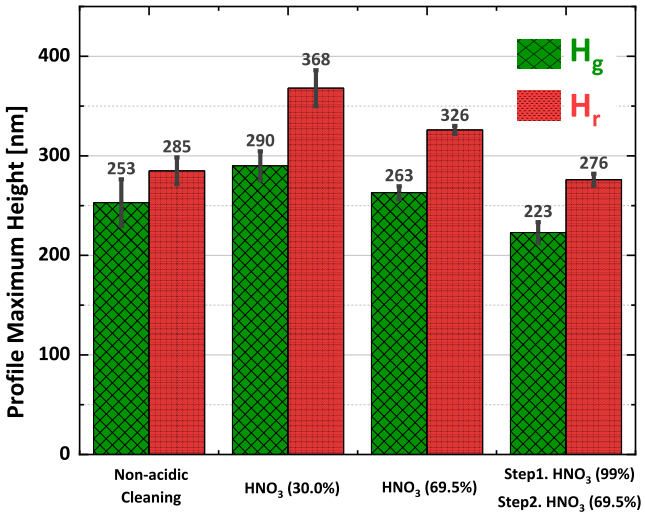

Figure 12. Influence of different cleaning methods on the hexagonal texture height. The G-axis height (H_g) and the R-axis height (H_r) are plotted. The standard deviation represents uniformity across the wafer surface area.

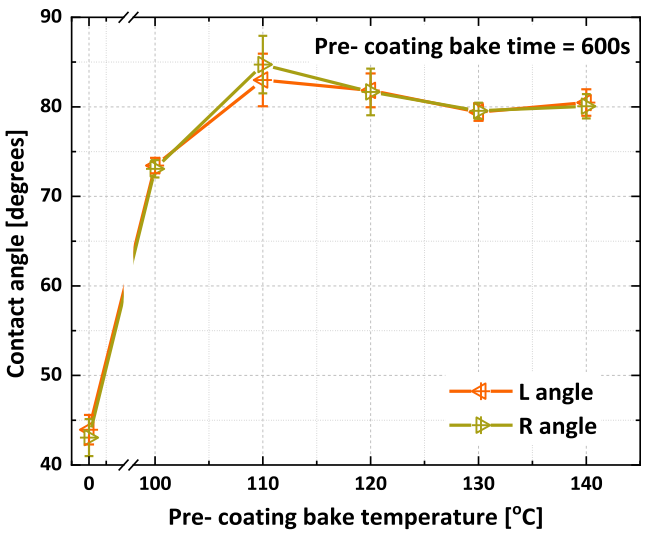

Figure 13. Variation of the contact angle with the precoating bake temperature (contact angles at the left (L) and right (R) sides of the water droplet).

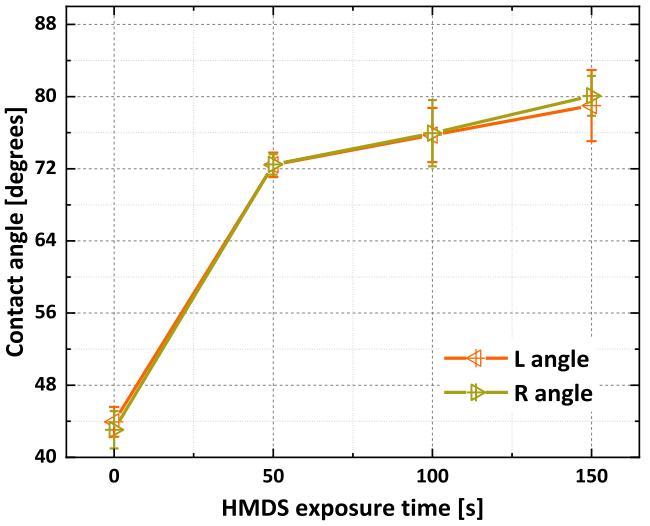

Figure 14. Variation of the contact angle with the HMDS exposure duration (contact angle at the water droplet's left (L) and right (R) sides).

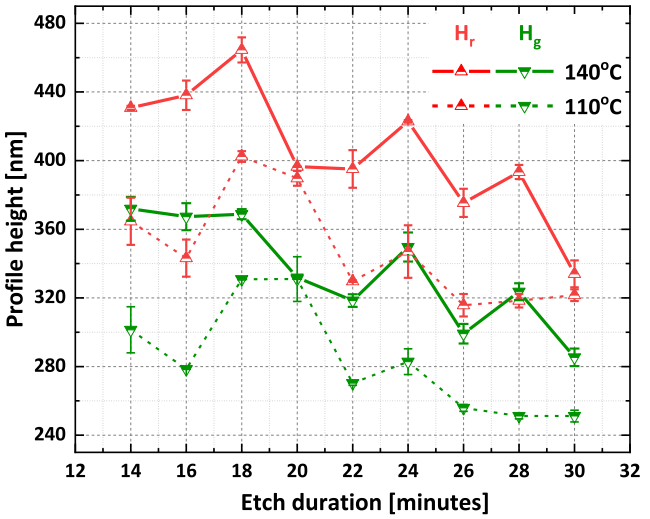

Figure 15. Influence of the hard bake temperature on the texture height. The G-axis height (H_g) and the R-axis height (H_r) are plotted for each time stamp.

This gradually decreases $H_r - H_g$ and starts flattening out the peaks.

https://doi.org/10.1021/acsaom.5c00328
ACS Appl. Opt. Mater. 2025, 3, 2360−2372

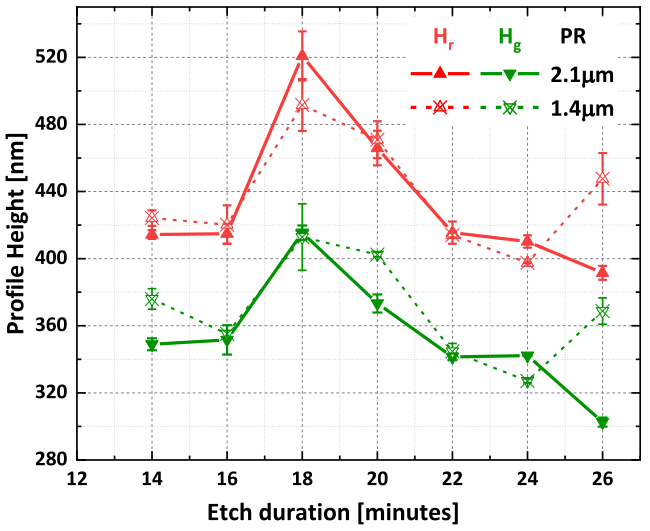

Figure 16. Influence of PR thickness on the texture height. The G-axis height (H_g) and the R-axis height (H_r) are plotted for each time stamp.

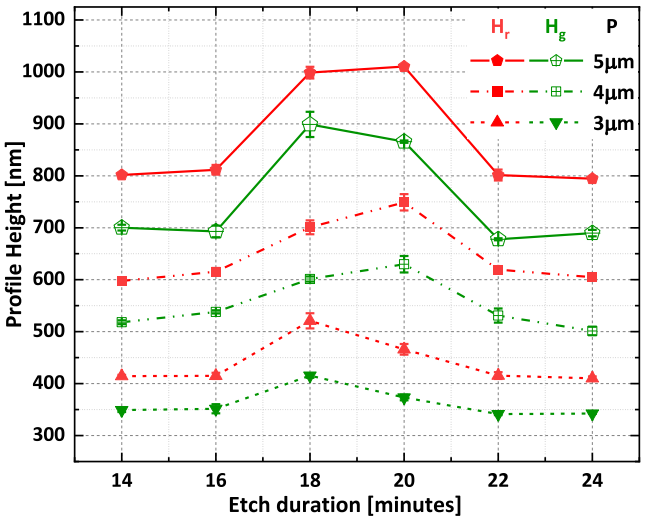

Figure 18. Influence of orifice periodicity on the texture height. The G-axis height (H_g) and the R-axis height (H_r) are plotted for each time stamp.

According to eq 1, for an orifice diameter of 1000 nm and a periodicity of 3000 nm, H_{exp} = 1230 nm. However, the H_r in baseline processing is 0.34 ± 0.01 μm, which is significantly smaller than the expected value. This diminishing height effect is caused by PR peel-off, as demonstrated schematically in Figure 11c. During the wet etching, the orifice diameter does not stay constant at 1000 nm, but increases with the etching duration. As the orifice diameter increases, the lateral etching is faster. Etching continues up to a critical level of the PR peel-off, causing a flat region at the base of the honeycomb. The SEM image of the texture shown in Figure 11a indicates this. Similar cases of flat bottoms are reported elsewhere in the making of hexagonal textures.[13,32,33] The PR peel-off is mainly determined by the adhesion of the PR to the glass surface.[44]

The D_e of baseline processing is 2.80 ± 0.02 μm. This implies that the effective diameter for etching is much higher than the intended diameter of 1.00 ± 0.01 μm. The corresponding $D_{e,P}$ is 0.80 ± 0.01, and the AR is 11.2 ± 0.1%.

Influence of the Cleaning Method

The effect of different cleaning steps on texture heights H_r and H_g is plotted in Figure 12. Acidic cleaning with a 30% HNO_3 solution shows an increase in H_r and $H_r - H_g$ values compared to the nonacidic baseline cleaning step. This implies that the nonacidic method is insufficient to clean the wafer surface. With an acid cleaning method, the adhesion between the PR and the glass is stronger.[38] As a result, the lateral etching is slowed, implying that the vertical depth will be higher by the time PR peels off. However, for glass substrates, a further increase in the concentration of the acidic bath from 30 to 69.5 and 99% HNO_3 decreases the texture height. The nitric acid cleaning affects the surface of Corning glass, altering the chemical composition of the glass,[49] combined with mild surface etching. This minute surface structure change can cause capillary action and pinning, changing material adhesion.[50] The local surface composition changes during acid etching

Table 1. Texture Height, Effective Orifice Diameter, and the Associated Parameters of Each Etching Duration Series Presented in This Manuscript

process	H_r [nm]	D_e [nm]	$D_{e,P}$ [-]	AR [%]
baseline	336 ± 4	2800 ± 15	0.80 ± 0.01	11.2 ± 0.1
hard baking 110 °C	370 ± 5	2720 ± 17	0.78 ± 0.02	12.3 ± 0.2
hard baking 140 °C	460 ± 8	2540 ± 20	0.73 ± 0.02	15.3 ± 0.3
PR thickness = 1.4 μm	491 ± 12	2480 ± 26	0.71 ± 0.02	16.3 ± 0.4
opt. recipe, P = 3 μm	521 ± 13	2420 ± 26	0.70 ± 0.03	17.3 ± 0.6
opt. recipe, P = 4 μm	748 ± 10	3120 ± 23	0.67 ± 0.01	18.8 ± 0.2
opt. recipe, P = 5 μm	1010 ± 3	3750 ± 14	0.65 ± 0.01	20.2 ± 0.1

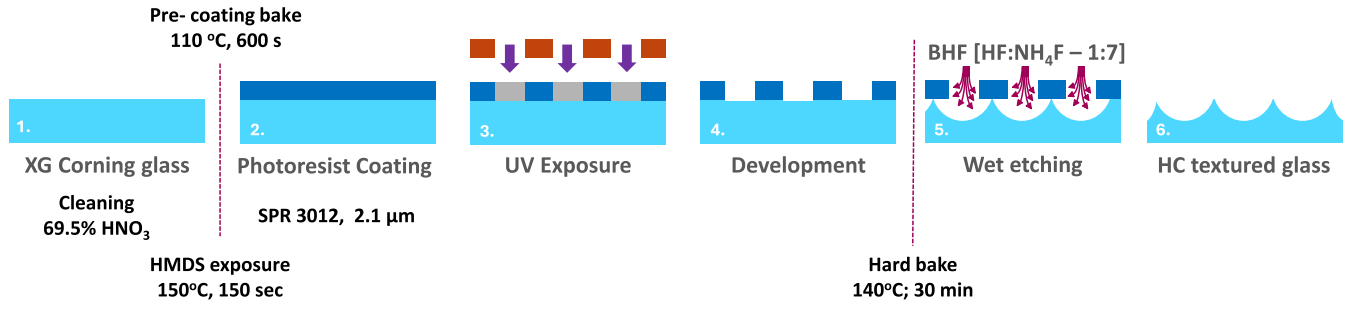

Figure 17. Schematic diagram of optimized processing steps involved in generating hexagonal textures on glass from the conducted experiments.

https://doi.org/10.1021/acsaom.5c00328
ACS Appl. Opt. Mater. 2025, 3, 2360−2372

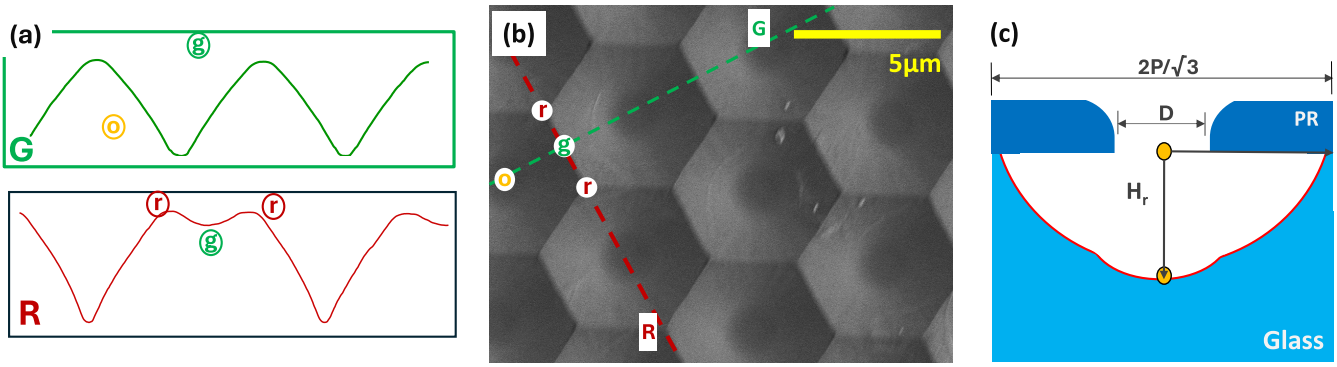

Figure 19. Honeycomb textures with optimized processing conditions (etching time of 20 min) with H_r = 1.010 ± 0.005 μm. (a) 2D surface profile along the G-axis and the R-axis, as extracted from AFM (the profiles are not to scale). (b) SEM image. The encircled letters are added to aid in interpreting the image. (c) Conceptual drawing of the cross-section with the hard-baked PR.

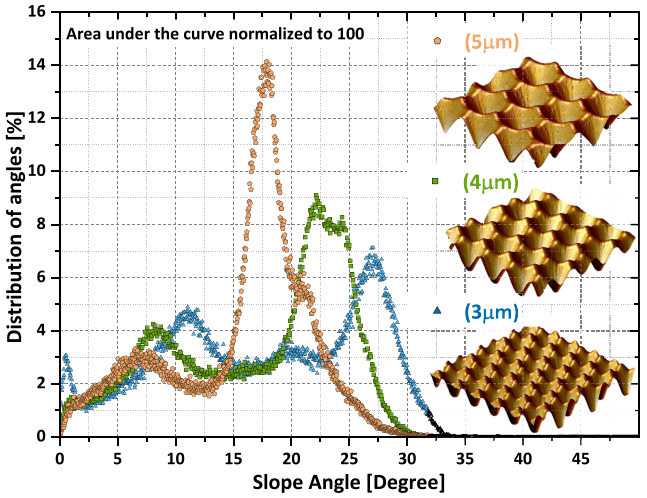

Figure 20. Distribution of surface vectors of the deepest obtained honeycomb texture for different periodicities in terms of the percentage of occurrence. The isometric view of AFM (scan size: 16 μm × 16 μm) is shown in the inset.

affect the surface free energy of the wafer. For concentrated baths, the composition changes are vigorous enough to affect the PR−glass adhesion negatively. This explains the decrease in the profile height.

Increasing the acidic concentration improves the uniformity of the texture over the substrate area. The standard deviation (σ) is 40 nm for 30% HNO_3 and 10 nm for 69.5% HNO_3. This would imply that the cleaning methodology based on 30% HNO_3 has a good adhesive nature, resulting in the deepest textures, but is insufficient to texture the 4 in. wafer area uniformly. For this reason, 69.5% HNO_3 is selected as an optimized condition in this work.

Influence of the Precoating Bake Temperature

Figure 13 represents the WCA measured for the glass wafer surface before HMDS exposure and PR coating at different pretreatment temperatures. The mean WCA peak value is at 85° for the samples precoat-baked at a temperature of 110 °C. For any temperature above 110 °C, physically absorbed hydroxyl groups are removed from the glass. In the optimized processing recipe, a temperature of 110 °C is used.

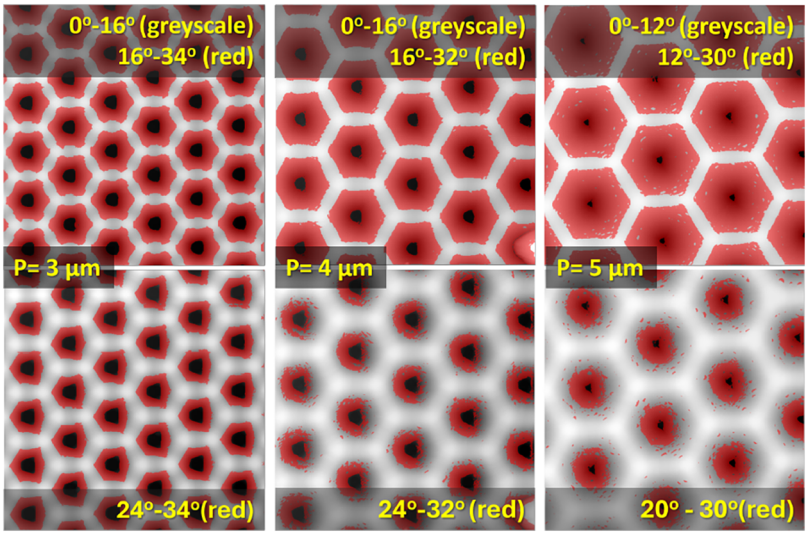

Figure 21. Surface slopes of honeycomb textures for different periodicities. The angle ranges in each image correspond to the peaks shown in Figure 20.

https://doi.org/10.1021/acsaom.5c00328
ACS Appl. Opt. Mater. 2025, 3, 2360−2372

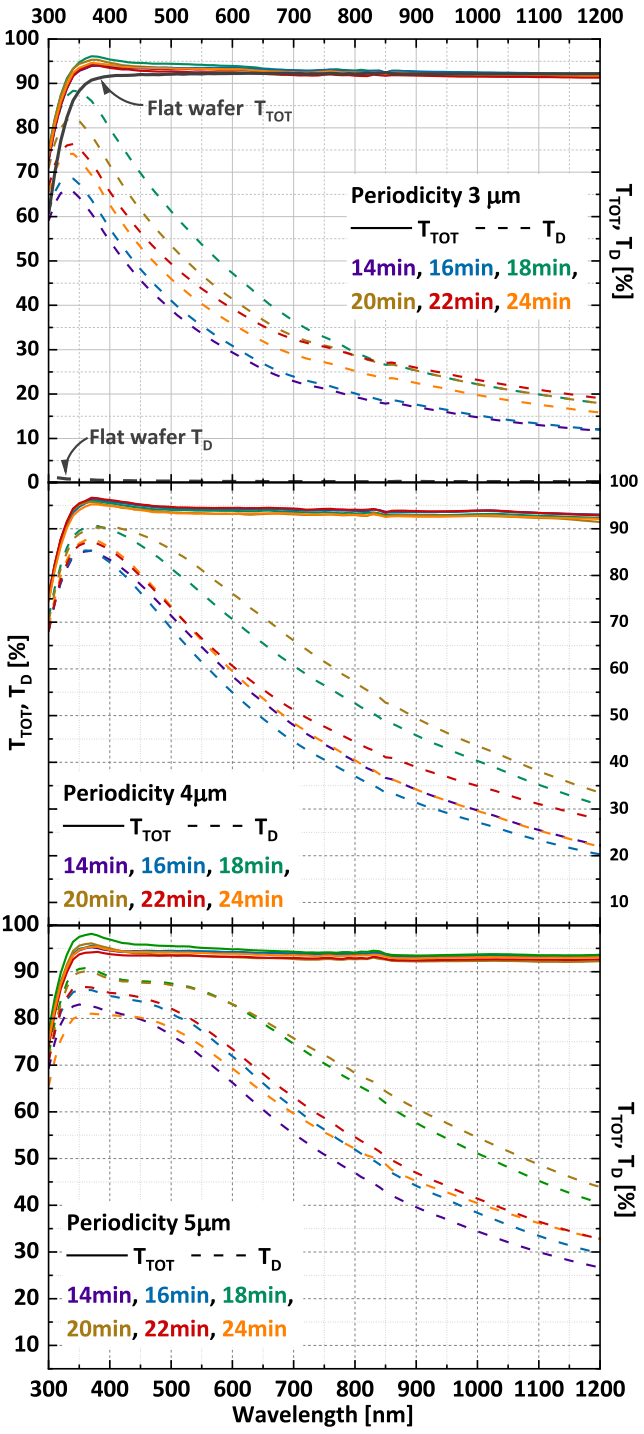

Figure 22. Total transmission (solid lines) and diffused transmission (dashed lines) spectra of hexagonal textures with periodicities of 3 μm (top), 4 μm (middle), and 5 μm (bottom). Each periodicity has six samples for an etching time of 14 to 24 min with 2 min intervals.

Influence of the HMDS Exposure Duration

Figure 14 shows the effect of the exposure duration on PR adhesion. The WCA of wafers primed with HMDS for different periods, from 50 to 150 s, in steps of 50 s at 130 °C, is depicted in the plot. Right after the wafer-cleaning step, without HMDS treatment, the WCA is 45°. However, the WCA increases with an increase in the exposure duration of HMDS, with a maximum value of 80° attained at 150 s of HMDS priming. The presence of nonpolar trimethylsilyl groups on the glass surface[51,52] decreases the wettability of the surface and, as a result, enhances PR adhesion to the glass.

Influence of the Hard Bake Temperature

After developing the coated PR, we observed that the hard baking of wafers results in a change in a pattern called "roundening". Around the reflow temperature, the PR softens, and the top surface of the PR changes to a blunt orifice border due to the evaporation of the PR from these parts.[47,48] The top diameter of orifices has become larger due to the rounding effect, channeling the etchant to the glass surface. Simultaneously, thermal cross-linking of the PR occurs at the PR–glass interface at elevated temperatures. Compared with baseline processing conditions, the texture height increases with hard baking.

Figure 15 indicates the texture height along the G- and R-axes obtained for different etch durations at 110 and 140 °C hard baking. After 18 min of etching in both hard bake conditions, the maximum texture height is attained. Hard baking at 140 °C results in a deeper texture than at 110 °C for all etch durations. Visually observed, the PR sediment inside the solution significantly reduces for hard-baked samples. This indicates the improved stability of the PR mask in the etchant.

The values of $D_{e,P}$ for hard baking at 110 and 140 °C are 0.78 ± 0.02 and 0.73 ± 0.02, respectively. The drop in $D_{e,P}$ implies that the etching is approaching an isotropic nature, forming the crater with a reduced PR peel-off. However, hard baking at such high temperatures can also result in crack formation in the PR, which could allow the etchant to seep in during the wet-etching process. This situation causes broken periodicity and unexpected spots on patterns on glass wafers.[48] Changes in the PR around the reflow temperatures can also shut off some orifices. After etching, such regions appear as unpatterned patches on the wafers. This is an aftereffect of the nonuniform heating of wafers.

Influence of PR Thickness

The samples prepared using the optimized recipe were etched for a time series with 2 min intervals ranging from 14 to 26 min. The variation of the texture height along the G- and R-axes for 2.1 and 1.4 μm PR thicknesses is shown in Figure 16. After 18 min of etching, the 2.1 μm PR coating makes deeper hexagons than the 1.4 μm PR coating. The gain in H_r is a consequence of the protected etching of the honeycomb edges, which is indicated by the same H_g of 1.4 and 2.1 μm thick PRs. We speculate that the thicker coating reduces the influx of etchant ions through the PR. The PR peel-off starts at 16 min of etching, but the thickness slows the effect. Beyond 18 min, the advantage of using a 2.1 μm PR vanishes as the hexagon formation is complete. At 20 min, the H_r value is the same for 1.4 and 2.1 μm thick PRs. This is because the etching is prominent for peaks at the R-axis and not for the crest of the G-axis. Other H_r and H_g values between 16 and 22 min coincide, indicating that the etch mechanism is the same once the hexagon formation is complete.

Another significant observation of this experiment is that using a 2.1 μm PR avoids unpatterned areas on wafers (caused as a result of hard baking of the 1.4 μm PR at elevated temperatures). This suggests that at a temperature of 140 °C, the 2.1 μm thick PR does not reflow to the extent that it affects the developed orifice pattern. The $D_{e,P}$ values of the process for the 1.4 μm and 2.1 μm PRs are 0.73 ± 0.02 and 0.71 ± 0.02, respectively.

https://doi.org/10.1021/acsaom.5c00328
ACS Appl. Opt. Mater. 2025, 3, 2360−2372

The optimized processing steps for generating hexagonal microtextures on glass are given in Figure 17.

Influence of Periodicity

Figure 18 shows the variation in height with the change in orifice periodicity. This figure shows that the profile height increases with the orifice periodicity. $H_r = 0.52 \pm 0.01$ μm for 3 μm periodicity, $H_r = 0.75 \pm 0.01$ μm for 4 μm periodicity, and $H_r = 1.010 \pm 0.005$ μm for 5 μm periodicity. This implies that the increase in periodicity plays a significant role in increasing the texture height. The increase of texture height with orifice periodicity across all of the etching durations is because point "r" is located farther away from orifice "o" when P increases. This can also explain why 2 extra minutes are required for complete honeycomb formation for orifice periodicities of 4 and 5 μm than for 3 μm.

The $D_{e,P}$ decreases as the periodicity increases. The $D_{e,P}$ value for 3 μm orifice periodicity is 0.70 ± 0.03; for 4 μm orifice periodicity, it is 0.67 ± 0.01; and for 5 μm orifice periodicity, it is 0.65 ± 0.01. The orifice periodicity of 5 μm gives a hexagonal texture with the highest aspect ratio of $20.2 \pm 0.1\%$ among all samples used in this study.

Sensitivity of Processes, $D_{e,P}$

The effective orifice diameter values, D_e and $D_{e,P}$, are recorded in Table 1. The magnitude of the drop of the $D_{e,P}$ value for a step implies the increase in isotropism imparted by the corresponding step. The final optimized recipe (refer Figure 17) changes the $D_{e,P}$ from 0.80 ± 0.01 to 0.73 ± 0.02, i.e., a decrease in $D_{e,P}$ by 0.10 ± 0.04. Hard baking is the critical parameter in this optimization, which contributed to 70% of this $D_{e,P}$ decrease. This implies that hard baking is the most critical step in the total process. Further, an increase in periodicity enhances isotropism involved in etching by approximately 3% for every 1 μm increase.

The AFM profile and SEM analysis of the honeycomb texture for an orifice periodicity of 5 μm developed with the optimized recipe are shown in Figure 19a,b. It shows that the hexagons have changed from craters with flat bases under the baseline recipe shown in Figure 11b,c to craters with curved bases under optimized processing conditions.

Potential of Hexagonal Textures on Glass

Figure 20 shows the distribution of surface angles of hexagonal microtextures made on glass with 3, 4, and 5 μm periodicities. The isometric views of the AFM scans are shown in the inset. The distribution of the surface normal values of hexagons shows two major peaks. As elaborated in Figure 21, the first peak occurring between 5 and 15° represents crater bases and honeycomb boundaries. This peak's intensity and absolute value combined represent the honeycombs' flatness. The second peak beyond the 15° angle represents the curved surface of the honeycomb textures. The intensity of this peak is representative of the steepness of the honeycomb. With an increase in the periodicity, both peaks shift toward smaller angles.

Figure 22 shows the total and diffuse transmittances corresponding to these samples. The total transmission (T_{TOT}) increases with periodicity, specifically for long wavelengths. Below 800 nm, a periodicity increase of 1 μm shows a gain of 1% in the total transmission. Beyond 850 nm, 4 and 5 μm periodicities show a similar transmission with a 2% increase compared to the 3 μm texture. The diffused transmittance (T_D) of hexagonal textures increases with periodicity. This observation correlates with the smaller surface angles of 5 μm hexagons. The hexagonal textures scatter short-wavelength light the best and show a drop in T_D for longer wavelengths. The drop is steepest for the 3 μm periodicity, followed by 4 and 5 μm periodicities, respectively. The diffusive nature of the hexagonal texture on glass depends on the crater height. It can be observed that the highest diffused transmittance spectra of each time series with μm, 4 and 5 μm periodicities correspond to the deepest sample in the set. In general, hexagonal features with higher periodicity values and deeper texture exhibit high optical transmission and scattering properties.

CONCLUSIONS

A detailed analysis of the processes used to make honeycomb textures in glass superstrates has been conducted. The influence of these processing parameters, especially their effect on texture depth, is studied in detail.

Glass wafer surfaces require acidic cleaning to facilitate proper adhesion between glass and the PR. This was done by cleaning the glass superstrates with 69.5% HNO_3 followed by a running water dip and spin-drying. Prebaking of wafers at 110 °C for 10 min before coating with the PR ensured the removal of any amount of adsorbed water from the surface. Additionally, it was noted that during the coating step, priming the surface with HMDS at 150 °C for 150 s best removes the polar hydroxyl groups to improve the surface adhesion toward the PR. Use of a 2.1 μm thick SPR3012 reduces the diffusion of the etchant ions through the PR. Postdevelopment, the samples were hard-baked at 140 °C for 30 min to enhance PR adhesion via cross-linking. Using these parameters, honeycombs were made on glass wafers with varying periodicities of 3, 4, and 5 μm. At 5 μm, hexagonal microtextures with a 1010 nm absolute depth are obtained.

Hexagonal texturing on glass does not exhibit perfectly isotropic etching, a property dedicated to the spatial distribution of the orifices. A parameter, $D_{e,P}$, is defined, successfully quantifying the extent of isotropism exhibited by the texturing process. The total transmission and scattering of light by hexagonal textures depend on their angle distribution. As the periodicity and height of the texture increase, hexagonal microtextures exhibit enhanced transmission and scattering properties.

In future publications, the optical performance of these substrates on solar cells will be reported.

AUTHOR INFORMATION

Corresponding Author

Govind Padmakumar − *Photovoltaic Materials and Devices, TU Delft, Delft 2628CD, The Netherlands;* orcid.org/0000-0001-7890-9511; Email: g.padmakumar@tudelft.nl

Authors

Aravind Balaji − *Photovoltaic Materials and Devices, TU Delft, Delft 2628CD, The Netherlands*

Matthias Criel − *Photovoltaic Materials and Devices, TU Delft, Delft 2628CD, The Netherlands*

Federica Saitta − *Photovoltaic Materials and Devices, TU Delft, Delft 2628CD, The Netherlands;* orcid.org/0009-0004-2120-2223

Gianluca Limodio − *Photovoltaic Materials and Devices, TU Delft, Delft 2628CD, The Netherlands*

https://doi.org/10.1021/acsaom.5c00328
ACS Appl. Opt. Mater. 2025, 3, 2360−2372

Paula Perez-Rodriguez − *Photovoltaic Materials and Devices, TU Delft, Delft 2628CD, The Netherlands*
René A. C. M. M. van Swaaij − *Photovoltaic Materials and Devices, TU Delft, Delft 2628CD, The Netherlands*
Arno H. M. Smets − *Photovoltaic Materials and Devices, TU Delft, Delft 2628CD, The Netherlands*

Complete contact information is available at: https://pubs.acs.org/10.1021/acsaom.5c00328

Notes

The authors declare no competing financial interest.

■ ACKNOWLEDGMENTS

The authors acknowledge financial and technical support from HyET Solar Netherlands B.V., Arnhem, The Netherlands. Additionally, the authors thank all technicians in the Else Kooi Laboratory for providing technical assistance with the processing of hexagons on glass, which is acknowledged.

■ REFERENCES

(1) Naresh, V.; Lee, N. A Review on Biosensors and Recent Development of Nanostructured Materials-Enabled Biosensors. *Sensors* **2021**, *21*, No. 1109.
(2) Koya, A. N.; Cunha, J.; Guo, T. L.; Toma, A.; Garoli, D.; Wang, T.; Juodkazis, S.; Cojoc, D.; Proietti Zaccaria, R. Novel Plasmonic Nanocavities for Optical Trapping-Assisted Biosensing Applications. *Adv. Opt. Mater.* **2020**, *8*, No. 1901481.
(3) Geng, Y.; Jang, J. H.; Noh, K. G.; Noh, J. H.; Lagerwall, J. P.; Park, S. Y. Through the Spherical Looking-Glass: Asymmetry Enables Multicolored Internal Reflection in Cholesteric Liquid Crystal Shells. *Adv. Opt. Mater.* **2018**, *6*, No. 1700923.
(4) Li, L.; Lin, H.; Qiao, S.; Huang, Y.-Z.; Li, J.-Y.; Michon, J.; Gu, T.; Alosno-Ramos, C.; Vivien, L.; Yadav, A.; Richardson, K.; Lu, N.; Hu, J. Monolithically integrated stretchable photonics. *Light:Sci. Appl.* **2018**, *7*, No. 17138.
(5) Li, Z.; Li, S.; Ma, T. Using Photonic Glasses as Colored Covers for Solar Energy Harvesting. *Adv. Opt. Mater.* **2023**, *11*, No. 2202370.
(6) Pan, C.; Chen, K.; Liu, B.; Ren, L.; Wang, J.; Hu, Q.; Liang, L.; Zhou, J.; Jiang, L. Fabrication of micro-texture channel on glass by laser-induced plasma-assisted ablation and chemical corrosion for microfluidic devices. *J. Mater. Process. Technol.* **2017**, *240*, 314−323.
(7) Yang, G.; van Swaaij, R. A.; Tan, H.; Isabella, O.; Zeman, M. Modulated surface textured glass as substrate for high efficiency microcrystalline silicon solar cells. *Sol. Energy Mater. Sol. Cells* **2015**, *133*, 156−162.
(8) Isabella, O.; Krč, J.; Zeman, M. Modulated surface textures for enhanced light trapping in thin-film silicon solar cells. *Appl. Phys. Lett.* **2010**, *97*, No. 101106.
(9) Tan, H.; Moulin, E.; Si, F. T.; Schüttauf, J.-W.; Stuckelberger, M.; Isabella, O.; Haug, F.-J.; Ballif, C.; Zeman, M.; Smets, A. H. M. Highly transparent modulated surface textured front electrodes for high-efficiency multijunction thin-film silicon solar cells. *Prog. Photovoltaics: Res. Appl.* **2015**, *23*, 949−963.
(10) Despeisse, M.; Battaglia, C.; Boccard, M.; Bugnon, G.; Charrière, M.; Cuony, P.; Hänni, S.; Löfgren, L.; Meillaud, F.; Parascandolo, G.; Söderström, T.; Ballif, C. Optimization of thin film silicon solar cells on highly textured substrates. *Phys. Status Solidi A* **2011**, *208*, 1863−1868.
(11) Fejes Tóth, L. *Regular Figures*; Elsevier, 2014.
(12) Hales, T. C. The Honeycomb Conjecture. *Discrete Comput. Geom.* **2001**, *25*, 1−22.
(13) De Vrijer, T.; Wiering, M.; Van Nijen, D.; Padmakumar, G.; Sambamurthy, S.; Limodio, G.; Smets, A. H. The optical performance of random and periodic textured mono crystalline silicon surfaces for photovoltaic applications. *EPJ Photovoltaics* **2022**, *13*, No. 23.
(14) Chou, S. Y.; Krauss, P. R.; Renstrom, P. J. Nanoimprint lithography. *J. Vac. Sci. Technol., B:Microelectron. Nanometer Struct.–Process., Meas., Phenom.* **1996**, *14*, 4129−4133.
(15) Russo, R. E.; Mao, X.; Yoo, J.; Gonzalez, J. *Laser-Induced Breakdown Spectroscopy*; Elsevier, 2007; pp 41−70.
(16) Moreau, W. M. *Semiconductor Lithography*; Springer US: Boston, MA, 1988.
(17) Guo, L. Nanoimprint Lithography: Methods and Material Requirements. *Adv. Mater.* **2007**, *19*, 495−513.
(18) Hauser, H.; Michl, B.; Schwarzkopf, S.; Kübler, V.; Müller, C.; Hermle, M.; Bläsi, B. Honeycomb texturing of silicon via nanoimprint lithography for solar cell applications. *IEEE J. Photovoltaics* **2012**, *2*, 114−122.
(19) Eisenhauer, D.; Sai, H.; Matsui, T.; Köppel, G.; Rech, B.; Becker, C. Honeycomb micro-textures for light trapping in multi-crystalline silicon thin-film solar cells. *Opt. Express* **2018**, *26*, A498−A507.
(20) Wang, Y.; Ke, C.; Wu, T.; Zhao, X.; Wang, R. Nanosecond laser texturing with hexagonal honeycomb micro-structure on Titanium for improved wettability and optical properties. *Optik* **2019**, *192*, No. 162953.
(21) Ehrfeld, W.; Schmidt, A. Recent developments in deep x-ray lithography. *J. Vac. Sci. Technol., B:Microelectron. Nanometer Struct.–Process., Meas., Phenom.* **1998**, *16*, 3526−3534.
(22) Kovačević, K.; Zhao, Y.; Procel, P.; Cao, L.; Mazzarella, L.; Isabella, O. Interdigitated-back-contacted silicon heterojunction solar cells featuring novel MoO_x -based contact stacks. *Prog. Photovoltaics: Res. Appl.* **2025**, *33*, 209−218.
(23) Miyajima, H.; Mehregany, M. High-aspect-ratio photolithography for MEMS applications. *J. Microelectromech. Syst.* **1995**, *4*, 220−229.
(24) Zhao, J.; Wang, A.; Green, M. A.; Ferrazza, F. 19.8% efficient "honeycomb" textured multicrystalline and 24.4% monocrystalline silicon solar cells. *Appl. Phys. Lett.* **1998**, *73*, 1991−1993.
(25) Zhao, J.; Wang, A.; Campbell, P.; Green, M. A 19.8% efficient honeycomb multicrystalline silicon solar cell with improved light trapping. *IEEE Trans. Electron Devices* **1999**, *46*, 1978−1983.
(26) Manea, E.; Budianu, E.; Purica, M.; Cernica, I.; Babarada, F. Technological process for a new silicon solar cell structure with honeycomb textured front surface. *Sol. Energy Mater. Sol. Cells* **2006**, *90*, 2312−2318.
(27) Sai, H.; Matsui, T.; Matsubara, K.; Kondo, M.; Yoshida, I. 11.0%-Efficient Thin-Film Microcrystalline Silicon Solar Cells With Honeycomb Textured Substrates. *IEEE J. Photovoltaics* **2014**, *4*, 1349−1353.
(28) Sai, H.; Saito, K.; Hozuki, N.; Kondo, M. Relationship between the cell thickness and the optimum period of textured back reflectors in thin-film microcrystalline silicon solar cells. *Appl. Phys. Lett.* **2013**, *102*, No. 053509.
(29) Gupta, P. K. Non-crystalline solids: glasses and amorphous solids **1996** *195* 158 164 .
(30) Sahu, V.; Vardhan, R. V.; Dewangan, P.; Srivastava, Y. K.; Pal, P. Wet bulk micromachining of Borofloat glass towards the fabrication of through-holes in different concentrations of hydrofluoric acid. *Int. J. Appl. Glass Sci.* **2025**, *16*, No. e70004, DOI: 10.1111/ijag.70004.
(31) Sahu, V.; Dewangan, P.; Vardhan, R. V.; Menon, P. K.; Pal, P. Fabrication of microchannels and through-holes in Borofloat glass using Cr thin film with positive photoresist as the masking layer through wet etching. *Mater. Today Commun.* **2024**, *41*, No. 110352, DOI: 10.1016/j.mtcomm.2024.110352.
(32) Park, H.; Iftiquar, S. M.; Shin, M.; Kim, H.; Jung, J.; Kim, S.; Le, A. H. T.; Kim, Y.; Pham, D. P.; Jeong, J.-S.; Yi, J. Fabrication of honeycomb textured glass substrate and nanotexturing of zinc oxide front electrode for its application in high efficiency thin film amorphous silicon solar cell. *J. Photonics Energy* **2017**, *7*, No. 025502.
(33) Park, H.; Kim, D. Influence on the Haze Effect of Si Thin-Film Solar Cell on Multi-Surface Textures of Periodic Honeycomb Glass. *Trans. Electr. Electr. Mater.* **2021**, *22*, 80−90.

(34) Sai, H.; Saito, K.; Kondo, M. Enhanced photocurrent and conversion efficiency in thin-film microcrystalline silicon solar cells using periodically textured back reflectors with hexagonal dimple arrays. *Appl. Phys. Lett.* **2012**, *101*, No. 173901.
(35) Corning Incorporated. Semiconductor Glass Wafers Product Information Sheet. 2015.
(36) Corning Incorporated. Exceptional Dimensional Stability and Surface Quality in Thin, Large-Size Sheets. 2021.
(37) Ge, Z.; Yang, H.; Li, La.; Lim, J.-S.; Prasanna Venkatesh, R.; Park, J.-G.; Pacco, A.; Halder, S. Evolution of Silicon wafer cleaning technology. 1990; Vol. *137*, p 1887.
(38) MicroChemicals GmbH. Chapter 01 MicroChemicals -Fundamentals of Microstructuring Substrate Preparation. 2010.
(39) Collins, R.H.; Deverse, F. T. Process for improving photoresist adhesion. **1970**.
(40) MicroChemicals GmbH. Chapter 01 MicroChemicals -Fundamentals of Microstructuring Softbake. 2010.
(41) Merck Performance Materials GmbH. Technical Data Sheet AZ. 5214 E Photoresist.
(42) He, Y.; Hu, W.; Cui, B. Effect of Triton X-100 surfactant and agitation on tetramethylammonium hydroxide wet etching for microneedle fabrication. *J. Vac. Sci. Technol. B* **2024**, *42*, No. 053002.
(43) Shubhava, J. A.; Kannarpady, G. K.; Kale, S.; Prabhu, S.; Pinto, R. Chemical etching of glasses in hydrofluoric Acid: A brief review. *Mater. Today: Proc.* **2022**, 46−51.
(44) MicroChemicals GmbH. Chapter 01 MicroChemicals -Fundamentals of Microstructuring Wet chemical etching - basics. 2010.
(45) Hyeongsing, P.; Jae, H. C.; Jung, J. H.; Duy, P. P.; Le, A. H. T.; Yi, J.; et al. A Review of Wet Chemical Etching of Glasses in Hydrofluoric Acid based Solution for Thin Film Silicon Solar Cell Application. *Curr. Photovoltaic Res.* **2017**, 75−82.
(46) Rohm and Haas Electronic Materials. MEGAPOSITTM SPRTM3000 SERIES PHOTORESIST For Microlithography Applications. 2006.
(47) Microchemicals GmbH. Chapter 01 MicroChemicals - Fundamentals of Microstructuring Reflow of Photoresist. 2010.
(48) MicroChemicals GmbH. Chapter 01 MicroChemicals -Fundamentals of Microstructuring Hardbake, Reflow and DUV Hardening. 2010.
(49) Jang, H. K.; Chung, Y. D.; Whangbo, S. W.; Kim, T. G.; Whang, C. N.; Lee, S. J.; Lee, S. Effects of chemical etching with nitric acid on glass surfaces. *J. Vac. Sci. Technol., A* **2001**, *19*, 267−274.
(50) Zhu, Z.; Chen, Y.; Xu, Z.; Yu, Z.; Luo, X.; Zhou, J.; Tian, Y.; Jiang, L. Super-spreading on superamphiphilic micro-organized nanochannel anodic aluminum oxide surfaces for heat dissipation. *iScience* **2021**, *24*, No. 102334.
(51) Chodkowski, M.; Terpiłowski, K.; Pasieczna-Patkowska, S. Fabrication of transparent polysiloxane coatings on a glass support via the sol-gel dip coating technique and the effect of their hydrophobization with hexamethyldisilazane. *Physicochem. Probl. Miner. Process.* **2020**, *56*, 76−88.
(52) Dentinger, P. M.; Taylor, J. W. Importance of chemistry at the resist-wafer interface for mechanical and lithographic adhesion **1996**249 260.

https://doi.org/10.1021/acsaom.5c00328
ACS Appl. Opt. Mater. 2025, 3, 2360−2372